

Journal of Materials Chemistry A

Accepted Manuscript



This is an *Accepted Manuscript*, which has been through the Royal Society of Chemistry peer review process and has been accepted for publication.

Accepted Manuscripts are published online shortly after acceptance, before technical editing, formatting and proof reading. Using this free service, authors can make their results available to the community, in citable form, before we publish the edited article. We will replace this *Accepted Manuscript* with the edited and formatted *Advance Article* as soon as it is available.

You can find more information about *Accepted Manuscripts* in the [Information for Authors](#).

Please note that technical editing may introduce minor changes to the text and/or graphics, which may alter content. The journal's standard [Terms & Conditions](#) and the [Ethical guidelines](#) still apply. In no event shall the Royal Society of Chemistry be held responsible for any errors or omissions in this *Accepted Manuscript* or any consequences arising from the use of any information it contains.

Cite this: DOI: 10.1039/c0xx00000x

www.rsc.org/xxxxxx

ARTICLE TYPE

Flexible and all-solid-state supercapacitors with long-time stability constructed on PET/Au/polyaniline hybrid electrodes

Kun Zhang,^{a,b} Haibo Hu^{*b}, Weitang Yao^a and Changhui Ye^{*b}

Received (in XXX, XXX) Xth XXXXXXXXX 20XX, Accepted Xth XXXXXXXXX 20XX

DOI: 10.1039/b000000x

In this work, symmetrical, flexible, and all-solid-state supercapacitors based on Au/polyaniline hybrid electrodes that are integrated on flexible polyethylene terephthalate substrates have been fabricated. The as-obtained supercapacitors acquire a maximum areal capacitance of 51.7 mF cm^{-2} at a current density of 0.1 mA cm^{-2} and a maximum energy density of 5.57 mWh cm^{-3} at the power density of 0.33 W cm^{-3} , both of which are comparable to the values obtained for other currently available flexible and all-solid-state supercapacitors. In addition, the supercapacitors have excellent flexibility when they are bent to 90° with the CV curve remaining almost unchanged, and superior cycling stability with the capacitance retention of 92.3% after 1000 cycles. Moreover, the supercapacitors have good corrosion resistance and long-time stability, of which the capacitive performance has almost no change after leaving in air atmosphere for two months or dipping in the acid or alkali solution for 24 h. With these superior features, the supercapacitors hold great promise to be used in portable/wearable electronics.

Introduction

The tremendously increasing power and energy demands for next-generation hand-held and flexible electronic devices such as roll-up displays, self-powered sensor networks, and wearable devices, has promoted the development for high-performance energy storage.¹⁻¹⁰ Supercapacitors (SCs) are the state-of-the-art energy storage devices that are superior to conventional lithium ion batteries in power density, and have higher energy density compared with traditional capacitor.¹¹ In addition, SCs have many other advantages such as small size, light-weight, ease of handling, wide range of operation temperatures, long life cycles, short charging time, low-cost, safety and environmental benignancy.¹² Therefore, SCs hold great promise as a competitive candidate for next-generation energy storage device with high-performance.¹³

Compared with conventional SCs using liquid electrolyte, all-solid-state supercapacitors integrating electrodes, solid electrolyte and separator to a solid whole, have many obvious advantages such as lightweight, high flexibility and high safety.¹⁴⁻

¹⁶ For example, due to the use of solid electrolyte, the all-solid-state SCs can effectively avoid the short circuit caused by the leakage of electrolyte. In addition, there is no additional packaging materials are used, and the fabrication of all-solid-state SCs does not involve complicated post-processing, which simplifies the preparation process and reduces the weight of the device. Finally, the flexible and all-solid-state SCs possess more excellent mechanical properties and could facilitate the integration with micro-sensors and micro-electronics to be powered. Therefore, the flexible and all-solid-state SCs have

become a research emphasis of flexible energy storage devices, and have great potential as new energy storage device for flexible, safe, and wearable electronics.¹⁷⁻²⁰

Generally speaking, all-solid-state SCs include electrodes, solid electrolyte and separator. Construction of flexible and all-solid-state SCs is first to grow active materials on flexible substrate to obtain the electrodes, and then stack two thin film electrodes with separator/solid-electrolyte in between.²¹⁻²⁴ However, the state-of-the-art flexible supercapacitors generally use the flexible electrodes in the form of carbon networks or fabric-carbon composites as main infrastructure to reserve the flexibility. Without the carbon networks or fabric-carbon composites, pseudocapacitive materials can barely be used to fabricate the flexible electrodes, so as to assemble the flexible supercapacitors. For example, Zhou and Chen et al. have fabricated high-performance flexible supercapacitors based on single-walled carbon nanotube/polyaniline films and the specific capacitance of hybrid film with 30 s polyaniline deposition time can achieve about 236 F g^{-1} .²⁵ Wei et al. designed a flexible supercapacitor based on a composite electrode combined cloth-supported SWCNTs and PANI nanowire arrays. The PANI/SWCNT/cloth composite electrode showed a higher capacitance of 410 F g^{-1} .²⁶ Chai and his group have prepared a kind of stretchable all-solid-state supercapacitor with wavy shaped PANI/grapheme electrodes, and this all-solid-state supercapacitor exhibits a maximum specic capacitance of 261 F g^{-1} .²⁷ Sawangphruk and his colleagues reported a high-performance flexible and all-solid-state supercapacitors based on silver nanoparticle-polyaniline-graphene nanocomposites coated on flexible carbon fiber. At an applied current density of 1.5 A g^{-1}

the supercapacitors exhibit a high specific capacitance of 828 F g⁻¹.²⁸ These reported SCs based on these flexible electrodes possess excellent flexibility and electrochemical performance. However, because of the high price, complicated preparation process and low preparation efficiency, the large-scale preparation of the SCs based on flexible conductive infrastructure fabricated with these carbon materials or carbon composites is still a problem. Moreover, the poor mechanical properties and corrosion resistance of some flexible substrate such as fabric limit its application, especially in the harsh environment. Therefore, more work is still needed to simplify the fabrication of flexible conductive infrastructure and to improve the performance of flexible and all-solid-state SCs.

In recent years, pseudocapacitive materials,^{29,30} for which the capacitance steps from a fast reversible faradic process of redox-active reaction, have received increasing attention because they can provide much higher specific capacitances than that from electric double layer capacitors arising from charge separation at the interface of electrolyte. Among the pseudocapacitive materials, polyaniline (PANI) is considered as one of the most promising electrode materials due to its low cost, ease of synthesis, relatively high theoretical capacity, and flexibility.³¹⁻³³

Herein, we introduced a simple method to construct symmetrical, flexible, and all-solid-state SCs, which is integrated on flexible polyethylene terephthalate film. In this method, the flexible PET films deposited Au served as a flexible scaffold and current collector, the PANI networks directly electrodeposited on Au current collectors served as electrode materials, and the PVA/H₂SO₄ gel electrolyte served as the binder and solid state electrolyte. The method obviates the need for fabricating the flexible electrodes in the form of carbon networks or fabric-carbon composites as main infrastructure to reserve the flexibility, which is a cumbersome and time-consuming work. The usage of Au electrode will not substantially increase the production cost compared to other electrodes. In addition, this method allows for the fabrication of SCs without the use of any organic binders, conductive additives or polymer separators, thus leading to good electrochemical performance because of the ease with which ions can access the active material. Finally, because of the excellent properties such as flexibility, durability, and resistance to corruptions, the PET film deposited Au not only shows excellent flexibility and conductivity, but also excellent corrosion resistance in the aqueous electrolytes, which is beneficial for protecting the flexible device from corroding by outermost chemical environment and improving the lifetime of the flexible device. With these unique advantages, such designed SCs exhibit good energy and power densities as well as an impressive long-term cycling stability and corrosion resistance, and hold great promise to be used in portable/wearable electronics.

Experimental

Fabrication of the Au/PANI hybrid electrodes on PET film

All chemicals were analytical grade and were used without

further purification. A piece of clean PET film was cut into the shape on demand, on which a thin film of gold (80 nm) was deposited by an electron beam evaporation system serving as the current collector. Then active materials (PANI nanowire networks) were in-situ electrodeposited on the surface of Au layers by oxidation of aniline (0.3 M in 1 M HCl aqueous solution) through a two-step method by a conventional three-electrode system. For the first step, the seeding layer of PANI was nucleated at a potential of 0.8 V for 60 s at room temperature. Then the nanowire networks were grown under constant current density of 2 mA cm⁻².

Fabrication of the flexible and all-solid-state SCs

A PVA/H₂SO₄ gel electrolyte was prepared by adding PVA power (6 g) into H₂SO₄ aqueous solution (6 g H₂SO₄ into 60 mL deionized water), and then heating the mixture to around 85 °C under vigorous stirring until the solution became clear (about 2 h). After cooling down, the gel was dropwise added onto two flexible PET/Au/PANI electrodes, and assembled the two PET/Au/PANI electrodes into a supercapacitor 30 min later. The PVA/H₂SO₄ gel membrane in the middle of two electrodes worked as both the solid electrolyte and separator. In order to vaporize the excess water, the as-fabricated device was left in the fume hood at room temperature for 24 h. Finally, the edge of the SCs was sealed with polydimethylsiloxane (PDMS) (Sylgard184).

Sample characterization

The morphology of samples was probed by scanning electron microscopy (SEM; JSM-6700M). The attenuated total reflection Fourier transform infrared spectroscopy (ATR-FTIR) of the electrodeposited PANI networks on Au layer was obtained using a Magna-IR 750 spectrometer in the range of 700-1400 cm⁻¹ with a resolution of 4 cm⁻¹. The Raman spectrum was taken on a LABRAM-HR confocal laser micro-Raman spectrometer using an Ar⁺ laser with the 514.5-nm line at room temperature. Cyclic voltammetry (CV), electrochemical impedance spectroscopy (EIS), and galvanostatic charge-discharge (GCD) measurements of MSCs were carried out on electrochemical workstation (IM6ex, Zahner). Impedance spectroscopy measurements were performed at open circuit voltage with ±10mV amplitude. A Panasonic DMC-FX3 digital camera was used to capture all the optical images.

Results and Discussions

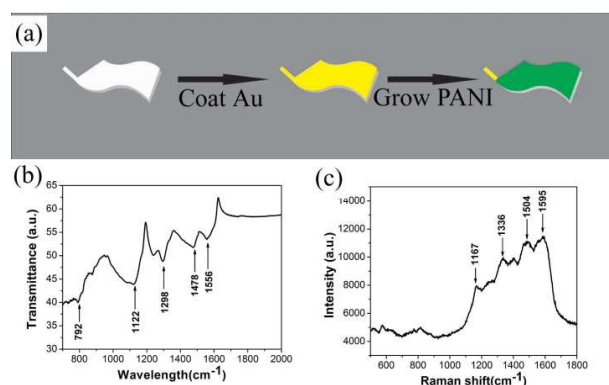


Fig. 1 (a) The diagrammatic drawing of fabrication process of PAP electrode; The ATR-FTIR spectrum (b) and Raman spectra (c) of the electrodeposited PANI networks on Au layer.

The schematic drawing of the fabrication process of Au/polyaniline hybrid electrodes integrated on PET film is shown in Fig. 1a. A common PET film is used as flexible substrates, on which an 80 nm thick Au film was deposited serving as the flexible current collector. PET is widely used as packaging materials for food and consumer products because of its excellent properties such as low-cost, flexibility, durability, and resistance to corrosions. Therefore, the PET film deposited Au shows excellent flexibility and corrosion resistance in the aqueous electrolytes, which is beneficial for improving the lifetime of the flexible device. Then PANI networks are grown through electrodeposition to obtain the PET/Au/PANI (PAP) hybrid electrodes. The chemical composition of the deposited PANI networks on Au layer was characterized by attenuated total reflection Fourier transform infrared spectroscopy (ATR-FTIR) and Raman spectra, and the results are shown in Fig. 1b and 1c. For ATR-FTIR, the bands at 1556 and 1478 cm^{-1} are assigned to C=C stretching vibrations of quinoid and benzenoid rings, respectively. The bands at 1298, 1122, and 792 cm^{-1} originate from C-N, C=N, and C-H stretching vibration, respectively.⁷ The Raman peaks at 1167, 1336, 1504, 1595 cm^{-1} are attributed to C-H bending vibration of quinoid rings, C-N stretching vibration, N-H bending vibration and the C=C bending vibration of benzenoid rings, respectively.³³ These results directly prove that PANI has been successfully deposited on the Au layer.

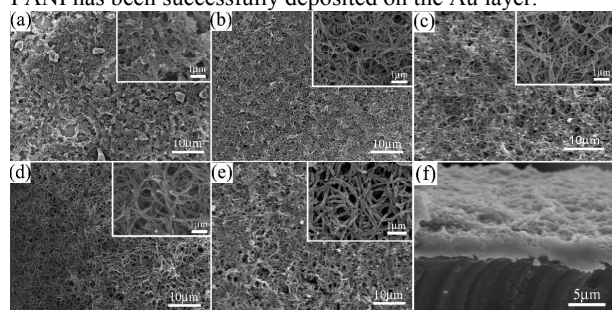


Fig. 2 SEM images for PANI deposited on PAP electrodes with different deposition time (a) 3 min, (b) 5 min, (c) 10 min, (d) 20 min, (e) 40 min, respectively. (f) The cross-section SEM images for PANI deposited on PAP electrodes with the deposition time of 5 min.

PAP hybrid electrodes with different PANI deposition time were firstly prepared to investigate the relation between electrochemical performance of the single PAP hybrid electrode and the deposition time. Fig. 2 shows the SEM images of PAP hybrid electrodes with different deposition time. As can be seen from Fig. 2, along with the increase of deposition time, the diameter of PANI nanowires tends to increase and PANI nanowires gradually form the network structure. However, if the deposition time is less than 3 min (Fig. 2a), PANI nanowires will not form a full network to cover the whole substrate. In the meantime, when the deposition time is too long and exceeds 40 min, PANI networks will accumulate seriously (Fig. 2e). Both are not conducive to the improvement of electrochemical

performance of PAP electrodes. Fig. 2f is a cross-section image of the deposited PANI nanowire network on the Au current collector (Fig. 2f), where the height of PANI network layer was about 3.0 μm for PAP with the deposition time of 5 min.

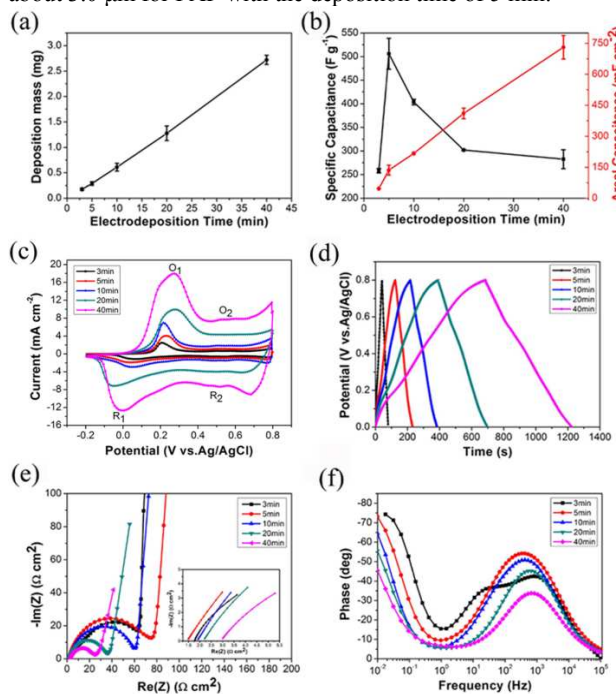


Fig. 3 Deposition mass (a), the total areal and specific capacitance (b) of the prepared single PAP electrode with respect to electrodeposition time of 3, 5, 10, 20, 40 min, respectively; (c) CV curves of PAP electrodes with different PANI deposition times at a constant scan rate of 10 mV s^{-1} ; (d) GCD curves of the PAP electrodes with different PANI deposition times at a constant current density of 1 mA cm^{-2} ; Nyquist plot (e) and Bode plot (f) of the PAP electrodes with different PANI deposition times.

To evaluate the electrochemical performance of PAP hybrid electrodes with different PANI deposition time, cyclic voltammetry (CV), galvanostatic charge-discharge (GCD), and electrochemical impedance spectroscopy (EIS) measurements were conducted in a three-electrode configuration in 1 M H_2SO_4 aqueous solution, and the results are shown in Fig. 3 and Fig. 4. Fig. 3c shows the CV curves of PAP electrodes with different deposition time at a constant scan rate of 10 mV s^{-1} , all of which show two obvious redox peaks that directly illustrate the pseudo-capacitive behaviour of the PAP hybrid electrodes (the pair of redox peaks O_1/R_1 was attributed to the redox transition of PANI between leucoemeraldine form and emeraldine form, and another pair of peaks O_2/R_2 is related to the emeraldine-pernigraniline transformation). The GCD curves of PAP hybrid electrodes with different PANI deposition time at a current density of 1 mA cm^{-2} were shown in Figure 3d. It can be observed that the charge and discharge time of PAP hybrid electrodes increased with PANI deposition time from 3 to 40 min. In the meantime, the mass loading of PANI also shows a linear increase with respect to deposition time under constant deposition current density of 2 mA cm^{-2} . As a result, the areal capacitance of PAP hybrid

electrodes increases with the mass loading of PANI at the same electrode area (1 cm^2), as indicated by the increases of the charge and discharge time. The areal capacitance with respect to different PANI masses is plotted versus the discharge current in Fig. 4a. As can be seen from Fig. 4a, along with the increase of deposition mass of PANI, the areal capacitance increases and the PAP electrode with the deposition time of 40 min exhibit the highest areal capacitance of about 802 mF cm^{-2} at the current density of 1 mA cm^{-2} (Fig. 3b and Fig. 4a). However, the average specific capacitance shows a downward trend after first rising, and reaches a maximum of about 475 F g^{-1} at the deposition time of 5 min with the discharge current of 1 mA cm^{-2} (Fig. 3b). As the redox reaction initiates at the surface layer of the pseudocapacitive materials in contact with the electrolyte, and is followed by the diffusion of the electrolyte ions inside the materials, a thick layer of PANI will slow ion diffusion from the electrolyte into the deeper parts of PANI network with deposition time increases, and thus generates a dead mass of PANI that does not take part in the redox reaction, thereby decreasing the capacitance per unit and leading to the above results. Even so, the obtained electrochemical results is still comparable to that of the above mentioned state-of-the-art flexible supercapacitors using the flexible electrodes in the form of carbon networks or fabric-carbon composites as main infrastructure to reserve the flexibility.²⁵⁻²⁷ The electrochemical performance of the PAP hybrid electrodes with different deposition times was further characterized by electrochemical impedance spectroscopy (EIS) measurements from 100 KHz to 10 mHz. As shown in Fig. 3e and 3f, the sample with deposition time of 3 min possesses two semicircles owing to its half-baked networks and incomplete coverage that will cause short circuit in the device. With the deposition time increase to beyond 5 min, the complete coverage of the substrate removes the diffusion process of electrolyte to the substrate and the low-frequency phase disappears for these samples. The equivalent series resistances (ESR) of PANI networks deposited for 3, 5, 10, 20 and 40 min are about 1.78, 1.5, 1.9, 2.2 and $3.0 \Omega \text{ cm}^2$, respectively. PAP hybrid electrode with the deposition time of 5 min (PAP-5 electrode) possesses the minimum ESR of $1.5 \Omega \text{ cm}^2$, which is of great importance since less energy and less power will be wasted to produce unwanted heat during the charge-discharge processes.

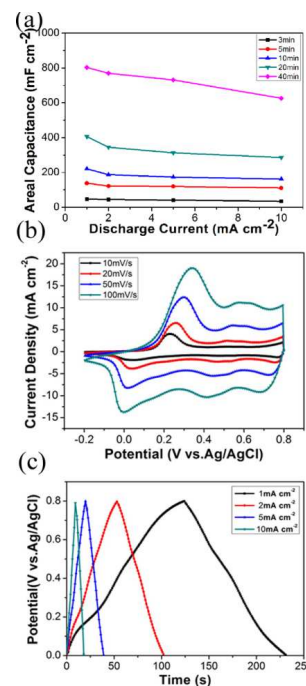


Fig. 4 (a) Areal capacitance of PAP electrodes with different PANI deposition time versus discharge current; (b) CV curves for PAP-5 electrode at different scan rates ranging from 10 to 100 mV/s ; (c) GCD curves of PAP-5 at different current density.

Based on above experimental results, PAP-5 electrode was selected as the typical electrode to conduct the further electrical property tests. Firstly, CV and GCD of single PAP-5 electrode were measured, and the results were shown in Fig. 4b and 4c, respectively. As can be seen from Fig. 4b, along with the increase of the scan rate, the peak current density increases but the shape still keeps the characteristics for an ideal pseudocapacitance. Moreover, the GCD curves at different current densities possess good symmetry and linear profile, also indicating the good capacitive performance of the single PAP-5 electrode (Fig. 4c). Considering practical applications, we further fabricated the symmetrical, flexible and all-solid-state SCs with PAP-5 electrodes sandwiching a PVA/ H_2SO_4 gel membrane as a separator between them. Fig. 5a is the diagrammatic drawing of the configuration of the fabricated symmetrical, flexible, and all-solid-state SCs based on PAP-5 electrode. To evaluate the electrochemical performance of the fabricated SCs device, CV scans of the SCs were performed from -0.8 V to 0.8 V ,³⁴ which possesses obvious couples of redox peaks attributed to redox transitions of PANI deposited on the electrodes and shows a highly symmetrical shape, indicating an ideal pseudocapacitive behaviour (Fig. 5d). Figure 5f shows the GCD curves of the device at different current densities. Both the symmetry and good linear profile of the charge and discharge curves indicated the good capacitive performance of the all-solid-state device. Areal capacitance (mF cm^{-2}) is calculated from the charge-discharge curves according to the following equations to evaluate the charge-storage capacity of the flexible and all-solid-state SCs based on PAP-5 electrode.^{35,36}

$$Cs = Q / \Delta ES = I \Delta t / \Delta ES \quad (1)$$

where C_s is the areal capacitance, Q is the total charge, I is the discharge current, Δt is the discharge time, ΔE is the potential window during the discharge process after IR drop, and S is the whole surface of the device. Fig. 6a shows the areal capacitance of the as-obtained flexible and all-solid-state SCs based on PAP-5 hybrid electrodes versus different discharge current. It can be seen that as the charge-discharge density decreases, the areal capacitance of the fabricated SC increases and can achieve a maximum areal capacitance of 51.7 mF cm^{-2} at the current density of 0.1 mA cm^{-2} . Even at a high current density of 2.0 mA cm^{-2} , the device can still acquire an areal capacitance of 32.75 mA cm^{-2} . In addition, because of the excellent mechanical flexibility of PET substrate, the all-solid-state device is highly flexible and the capacitance performance has little change even if the device is bent to about 90° (Fig. 5c and 5e). Moreover, the device can be connected in series to improve the output voltage to light a light-emitting diode (LED) (Fig. 5b). EIS measurement reveals the complete device has an ESR of about $10.23 \text{ } \Omega \text{ cm}^2$ (Fig. 5g), which is larger than that of single electrode.

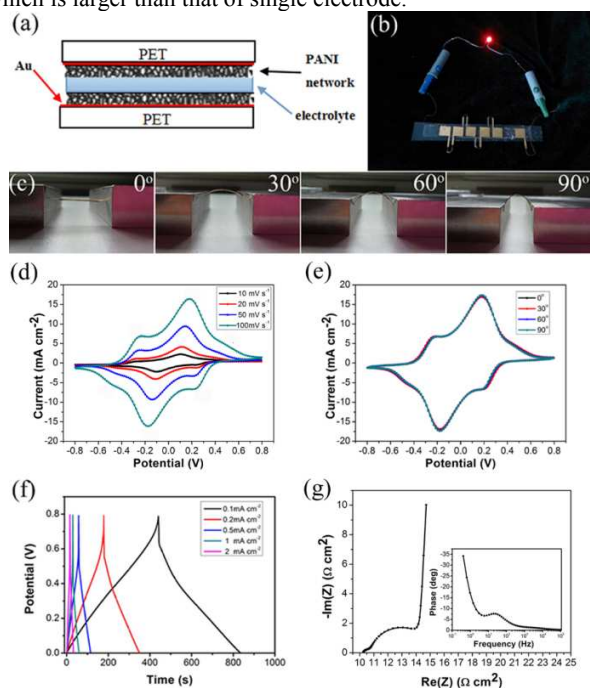


Fig. 5 (a) Schematic drawing of the SC fabricated with PAP-5; (b) The photograph of six all-solid-state SCs fabricated with PAP-5 connected in series to light a red LED; (c) The photographs of the flexible and all-solid-state SCs fabricated with PAP-5 at four bending states with bending angle of 0° , 30° , 60° and 90° , respectively; (d) CV curves for SC fabricated with PAP-5 at different scan rates ranging from 10 to 100 mV s^{-1} ; (e) CV curves of the SC fabricated with PAP-5 at the four bending states; (f) GCD curves of SC fabricated with PAP-5 at different current density; (g) Nyquist plot of the fabricated SC based on PAP-5 electrodes. The inset shows the Bode plot of the SC based on PAP-5 electrodes.

The discharged volumetric energy density W (Wh cm^3) and power density P (W cm^3) of the flexible and all-solid-state SCs were the crucial parameters for practical applications, which can

be calculated from these GCD curves through the following equations:

$$E = C \times (\Delta E)^2 / (2 \times 3600 \times V) \quad (2)$$

$$P = (\Delta E)^2 / 4R_{ESR}V \quad (3)$$

where E is the energy density (Wh cm^{-3}), P is the power density (W cm^{-3}), C is the total capacitance of the device, ΔE is the operating voltage window (the applied voltage excluding the voltage of iR drop), R_{ESR} is the internal resistance of the device ($R_{ESR} = V_{drop}/2i$), V is the polymer volume (cm^3).³⁷ As shown in Fig. 6b, the Ragone plot indicates that the fabricated device can acquire a maximum energy density of 5.57 mWh cm^{-3} at a power density of 0.33 W cm^{-3} and a maximum power density of 1.47 W cm^{-3} at an energy density of 2.46 mWh cm^{-3} . The Table 1 compares the volumetric power densities and energy densities of the device to the results for other flexible and all-solid-state energy storage devices, which shows that the electrochemical performance of the fabricated device is comparable to the values obtained for other currently available flexible and all-solid-state

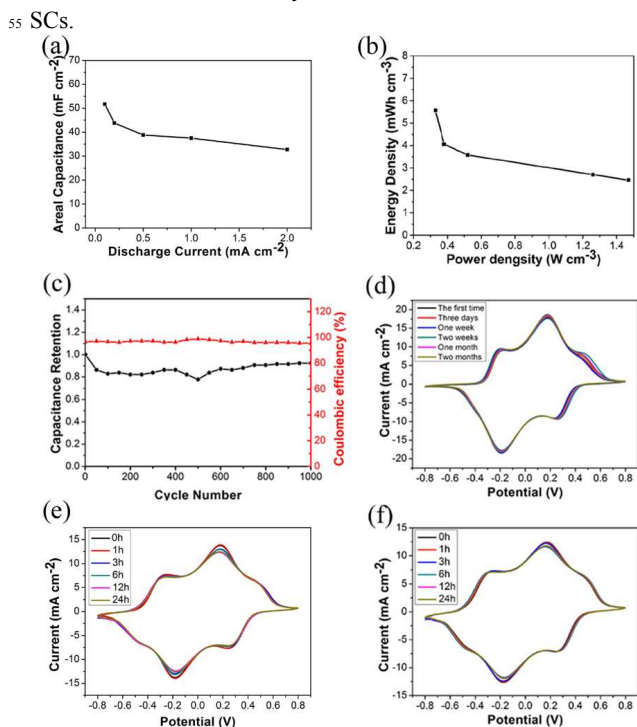


Fig. 6 (a) Areal capacitance of the SC fabricated with PAP-5 versus different discharge current; (b) Ragone plot for the SC fabricated with PAP-5; (c) Cycle performance and Coulombic efficiency of the all-solid-state SC at current density of 0.2 mA cm^{-2} over 1000 cycles. (d) CV scans of the SC fabricated with PAP-5 after placing 3 days, one week, two weeks, a month, two months, respectively, and CV scans of the SC fabricated with PAP-5 electrodes dipped in acid (e) and alkali (f) solution for 1, 3, 6, 12, 24 h, respectively.

As a potential energy storage device, the stability of the SCs must be examined. Firstly, the cycle stability of the fabricated SC was tested at a current density of 0.2 mA cm^{-2} for 1000 cycles. As shown in Fig. 6c, the capacitance of the device could remain

92.3% after 1000 cycles with respect to the first cycle, and the coulombic efficiency is about 98% during the whole 1000 cycles, indicating a good cycling stability of the as-obtained SCs. In addition, the long-term stability of the fabricated all-solid-state SCs was tested after three days, one week, two weeks, one month, two months, respectively. As shown in Fig. 6d, the CV curves of the fabricated device have almost no change, which reveals that the device also possesses good long-term stability. Moreover, the fabricated SCs possess excellent corrosion resistance. The fabricated SCs was immersed in an aqueous

H₂SO₄ (pH 1) or an aqueous KOH solution (pH 14) for 24 h, rinsed with water, and tested with CV. As shown in Fig. 6e and 6f, after strong acid or strong alkaline treatment, the CV curves remain almost unchanged, which shows the good corrosion resistance of the SCs.

Additionally, it is possible to utilize graphene as the electrode to improve the corrosion resistance of the SCs in future work, since graphene is well-documented for its chemical stability.

	Energy density	Power density	Ref.
PET/Au/MnO ₂ Electrodes-SCs	1.75 mWh cm ⁻³	3.44 W cm ⁻³	18
Polypyrrole-coated paper Electrodes-SCs	1 mWh cm ⁻³	0.27 W cm ⁻³	24
pencil-drawing graphite/PANI Electrodes-SCs	0.32 mWh cm ⁻³	0.054 W cm ⁻³	33
VN/CNT Hybrid Electrodes-SCs	0.54 mWh cm ⁻³	0.4 W cm ⁻³	36
PET/Au/PANI Electrodes-SCs	5.57 mWh cm ⁻³	0.33 W cm ⁻³	This work

Table 1. Typical results of other currently available flexible and all-solid-state SCs.

Conclusions

In summary, we have successfully fabricated flexible and high-performance all-solid-state SCs based on Au/polyaniline hybrid electrodes that are integrated on flexible polyethylene terephthalate substrates. The fabricated SCs acquire a maximum areal capacitance of 51.7 mF cm⁻² at a current density of 0.1 mA cm⁻² and a maximum energy density of 5.57 mWh cm⁻³ at the power density of 0.33 W cm⁻³, which are comparable to the values obtained for other currently available flexible and all-solid-state supercapacitors. In addition, the fabricated all-solid-state SCs have excellent mechanical flexibility, long-time stability, acid/alkaline-corrosion resistance, and can be connected in series to light-up a red light-emitting diode. This method is simple, environmentally benign and easy to be scaled up. The SCs fabricated with this method hold great promise to be used as flexible energy storage devices for portable and wearable electronics in the future.

Acknowledgments

This work was supported by National Basic Research Program of China (973 Program, Grant No. 2011CB302103), National Natural Science Foundation of China (Grant Nos. 11274308 and 21401202), Hundred Talent Program of the Chinese Academy of Sciences, and the Natural Science Foundation of Anhui Province for Outstanding Youth (No. 1108085J13).

Notes and references

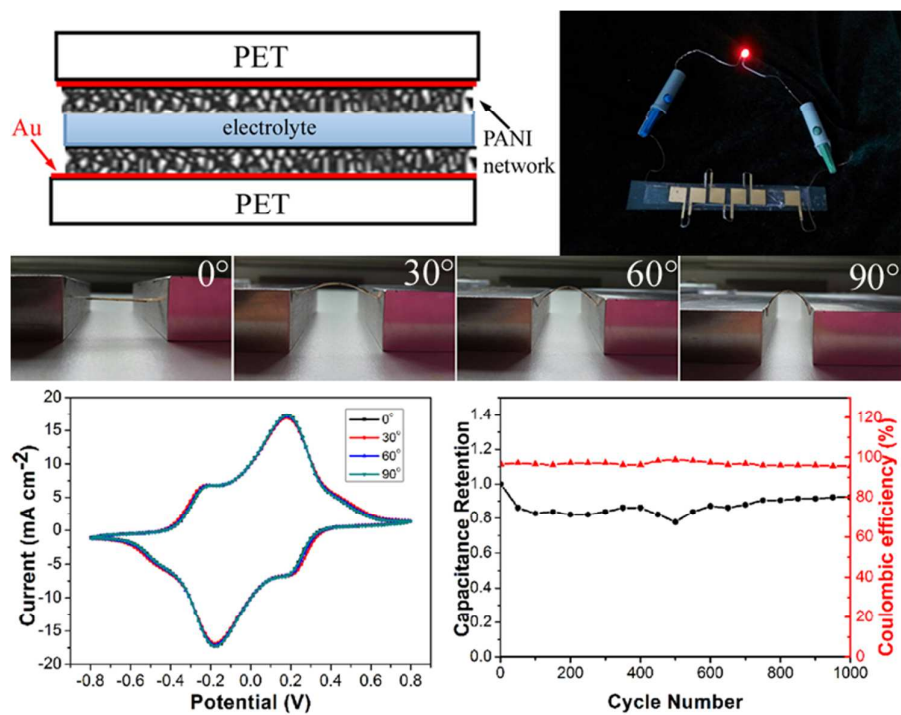
^aSchool of Materials Science and Engineering, Hefei University of Technology, Hefei 230039, China.

^bAnhui Key Laboratory of Nanomaterials and Technology, and Key Laboratory of Materials Physics, Institute of Solid State Physics, Chinese Academy of Sciences, Hefei 230031, China. Telephone: +86-551-65595629; Fax: +86-551-65591434; E-mail: chye@issp.ac.cn; haibohu@issp.ac.cn

- P. Simon, Y. Gogotsi, *Nat. Mater.*, 2008, **7**, 845-854.
- D. Pech, M. Brunet, H. Durou, P. Huang, V. Mochalin, Y. Gogotsi, P. L. Taberna, P. Simon, *Nat. Nanotechnol.*, 2010, **5**, 651-654.
- J. F. Ihlefeld, P. G. Clem, B. L. Doyle, P. G. Kotula, K. R. Fenton, C. A. Appleby, *Adv. Mater.*, 2011, **23**, 5663-5667.
- D. J. Lipomi, M. Vosgueritchian, B. C. Tee, S. L. Hellstrom, J. A. Lee, C. H. Fox, Z. Bao, *Nat. Nanotechnol.*, 2011, **6**, 788-792.
- X. Zhang, L. Gong, K. Liu, Y. Cao, X. Xiao, W. Sun, X. Hu, Y. Gao, J. Chen, J. Zhou, *Adv. Mater.*, 2010, **22**, 5292-5296.
- X. Xiao, L. Yuan, J. Zhong, T. Ding, Y. Liu, Z. Cai, Y. Rong, H. Han, J. Zhou, Z. L. Wang, *Adv. Mater.*, 2011, **23**, 5440-5444.
- L. Yuan, X. Xiao, T. Ding, J. Zhong, X. Zhang, Y. Shen, B. Hu, Y. Huang, J. Zhou, Z. L. Wang, *Angew. Chem. Int. Ed.*, 2012, **51**, 4934-4938.
- Y. Yang, S. Jeong, L. Hu, H. Wu, S. W. Lee, Y. Cui, *Proc. Natl. Acad. Sci. U.S.A.* 2011, **108**, 13013-13018.
- X. Lu, G. Wang, T. Zhai, M. Yu, J. Gan, Y. Tong, Y. Li, *Nano Lett.*, 2012, **12**, 1690-1696.
- L. Yuan, X. H. Lu, X. Xiao, T. Zhai, J. Dai, F. Zhang, B. Hu, X. Wang, L. Gong, J. Chen, *ACS Nano*, 2012, **6**, 656-661.
- X. Cai, M. Peng, X. Yu, Y. P. Fu, D. C. Zou, *J. Mater. Chem. C*, 2014, **2**, 1184-1200.
- M. Beidaghi and Y. Gogotsi, *Energy Environ. Sci.*, 2014, **7**, 867-884.
- X. H. Lu, M. H. Yu, G. M. Wang, Y. X. Tong, Y. Li, *Energy Environ. Sci.*, 2014, DOI: 10.1039/c4ee00960f.
- C. Meng, C. Liu, L. Chen, C. Hu, S. Fan, *Nano Lett.*, 2010, **10**, 4025-4031.
- M. Kaempgen, C. K. Chan, J. Ma, Y. Cui, G. Gruner, *Nano Lett.*, 2009, **9**, 1872-1876.
- Z. Weng, Y. Su, D.-W. Wang, F. Li, J. Du, H.-M. Cheng, *Adv. Energy Mater.*, 2011, **1**, 917-922.
- K. Wang, W. J. Zou, B. G. Quan, A. F. Yu, H. P. Wu, P. Jiang, Z. X. Wei, *Adv. Energy Mater.*, 2011, **1**, 1068-1072.
- W. P. Si, C. L. Yan, Y. Chen, S. Oswald, L. Y. Han, O. G. Schmid, *Energy Environ. Sci.*, 2013, **6**, 3218-3223.
- Y. P. Fu, X. Cai, H. W. Wu, Z. B. Lv, S. C. Hou, M. Peng, X. Yu, D. C. Zou, *Adv. Mater.*, 2012, **24**, 5713-5718.
- X. Xiao, T. Q. Li, P. H. Yang, Y. Gao, H. Y. Jin, W. J. Ni, J. Zhou, et al, *ACS Nano*, 2012, **6**, 9200-9206.
- F. H. Meng, Y. Ding, *Adv. Mater.*, 2011, **23**, 4098-4102.
- M. H. Yu, Y. X. Zeng, C. Zhang, X. H. Lu, C. H. Zeng, C. Z. Yao,

- Y. Y. Yang, Y. X. Tong, *Nanoscale*, 2013, **5**, 10806-10810.
23. Y. M. He, W. J. Chen, X. D. Li, Z. X. Zhang, J. C. Fu, C. H. Zhao, E. Q. Xie, *ACS Nano*, 2013, **7**, 174-182.
24. L. Y. Yuan, B. Yao, B. Hu, K. F. Huo, W. Chen, J. Zhou, *Energy Environ. Sci.*, 2013, **6**, 470-476.
25. Z. Niu, P. Luan, Q. Shao, H. Dong, J. Li, J. Chen, D. Zhao, L. Cai, W. Zhou, X. Chen, S. Xie, *Energy Environ. Sci.*, 2012, **5**, 8726-8733.
26. K. Wang, P. Zhao, X. Zhou, H. Wu and Z. Wei, *J. Mater. Chem.*, 2011, **21**, 16373-16378.
27. Y. Z. Xie, Y. Li, Y. D. Zhao, Y. H. Tsang, S. P. Lau, H. T. Huang, Y. Chai, *J. Mater. Chem. A*, 2014, **2**, 9142-9149.
28. M. Sawangphruk, M. Suksomboon, K. Kongsupornsak, J. Khuntilo, P. Srimuk, Y. Sanguansak, P. Klumbud, P. Suktha, P. Chiochan, *J. Mater. Chem. A*, 2013, **1**, 9630-9636.
29. S. Ghosh and O. Inganas, *Adv. Mater.*, 1999, **11**, 1214-1218.
30. L. L. Zhang, X. S. Zhao, *Chem. Soc. Rev.*, 2009, **38**, 2520-2531.
31. K. Wang, H. P. Wu, Y. N. Meng and Z. X. Wei, *small*, 2014, **10**, 14-31.
32. L. Nyholm, G. Nyström, A. Mihranyan and M. Strømme, *Adv. Mater.*, 2011, **23**, 3751-3769.
33. B. Yao, L. Y. Yuan, X. Xiao, J. Zhang, Y. Y. Qi, J. Zhou, J. Zhou, B. Hu, W. Chen, *Nano Energy*, 2013, **2**, 1071-1078.
34. X. Q. Jiang, S. Setodoi, S. Fukumoto, I. Imae, K. J. Komaguchi, J. Yano, H. Mizota, Y. Harima, *Carbon*, 2014, **67**, 662-672.
35. C. Guan, X. L. Li, Z. L. Wang, X. H. Cao, C. Soci, H. Zhang, and H. J. Fan, *Adv. Mater.*, 2012, **24**, 4186-4190.
36. X. Xiao, X. Peng, H.Y. Jin, T. Q. Li, C. C Zhang, B. Gao, B. Hu, K. F. Huo and J. Zhou, *Adv. Mater.*, 2013, **25**, 5091-5097.
37. M. F. El-Kady, V. Strong, S. Dubin, R. B. Kaner, *Science*, 2012, **335**, 1326.

The table of contents



Symmetrical, flexible, and all-solid-state supercapacitors based on Au/polyaniline hybrid electrodes integrated on flexible polyethylene terephthalate film are presented.